

# Weak gravitational shear and flexion with polar shapelets

Richard Massey<sup>1</sup>, Barnaby Rowe<sup>2</sup>, Alexandre Refregier<sup>3</sup>, David J. Bacon<sup>2</sup> & Joel Bergé<sup>3</sup>

<sup>1</sup> *California Institute of Technology, 1200 E. California Blvd., Pasadena, CA 91125, U.S.A.; rjm@astro.caltech.edu*

<sup>2</sup> *Institute for Astronomy, Blackford Hill, Edinburgh EH9 3HJ, U.K.*

<sup>3</sup> *Service d’Astrophysique, Bât. 709, CEA Saclay, F-91191 Gif sur Yvette, France*

Accepted —. Received —; in original form —.

## ABSTRACT

We derive expressions, in terms of “polar shapelets”, for the image distortion operations associated with weak gravitational lensing. Shear causes galaxy shapes to become elongated, and is sensitive to the second derivative of the projected gravitational potential; flexion bends galaxy shapes into arcs, and is sensitive to the third derivative. Polar shapelets provide a natural representation, in which both shear and flexion transformations are compact. Through this tool, we understand progress in several weak lensing methods. We then exploit various symmetries of shapelets to construct a range of shear estimators with useful properties. Through an analogous investigation, we also explore several flexion estimators. In particular, some of the estimators can be measured simultaneously and independently for every galaxy, and will provide unique checks for systematics in future weak lensing analyses. Using simulated images from the Shear TEsting Programme (STEP), we show that we can recover input shears with no significant bias. A complete software package to parametrize astronomical images in terms of polar shapelets, and to perform a full weak lensing analysis, is available on the world wide web.

**Key words:** methods: data analysis — techniques: image processing — gravitational lensing

## 1 INTRODUCTION

Weak gravitational lensing is a powerful method to map the distribution of mass in the Universe, regardless of its nature or state (for reviews see Mellier 1999; Bartelmann & Schneider 2001; Refregier 2003). The apparent shapes of background galaxies become distorted as their light travels near mass concentrations along their line of sight to the Earth. The well-known shearing of galaxies, in which intrinsically circular sources would be seen as elongated ellipses, is induced by an amount proportional to the second derivative of the projected gravitational potential. Such distortion has been measured around individual galaxy clusters (*e.g.* Wittman *et al.* 2001; Wittman *et al.* 2003; Bacon & Taylor 2003; Bradač *et al.* 2005; Wittman *et al.* 2006) and, in a statistical fashion, by large scale structure (recent measurements include Massey *et al.* 2004; Van Waerbeke *et al.* 2005; Heymans *et al.* 2005; Jarvis *et al.* 2005; Hoekstra *et al.* 2006; Semboloni *et al.* 2006; Hetterscheidt *et al.* 2006; Schrabback *et al.* 2006).

A higher-order effect, known as “flexion”, is also emerging as a probe of the distribution of mass on small scales, and particularly in the inner cores of galaxy clusters (Goldberg & Natarajan 2002; Irwin & Schmakova 2003; Goldberg & Bacon 2005; Bacon *et al.* 2006; Irwin & Schmakova 2006; Okura, Umetsu & Futamase 2006; Goldberg & Leonard 2006). Variation in the shear signal across the width of a background galaxy causes bending in its apparent shape.

This is the next term in a lensing expansion that leads towards the formation of an arc, as in strong lensing. The flexion is sensitive to the third derivative of the projected gravitational potential.

Precise image analysis techniques are required to detect weak gravitational lensing, because the shapes of galaxies are changed by the effect by only a few percent. In fact, the lensing contribution to the shape is about an order of magnitude smaller than the dispersion of galaxies’ intrinsic morphologies and the spurious distortions introduced by typical imperfections in telescopes. The widely used shear measurement method by Kaiser, Squires & Broadhurst (KSB, 1995) has been successful in many contexts, but contains several documented shortcomings: it is found to be insufficiently accurate to measure shears with a desired accuracy of less than 1% (*c.f.* Bacon *et al.* 2001; Erben *et al.* 2001; Heymans *et al.* 2005 (STEP1); Massey *et al.* 2006 (STEP2)), and it is mathematically ill-defined for realistic Point Spread Functions (*c.f.* Kaiser 2000; Kuijken 1999; Hirata & Seljak 2003).

Several new shear measurement methods are being developed, to fully exploit future space-based weak lensing surveys with HST or the proposed SNAP, DUNE or JDEM missions, and ground-based wide-field surveys such as those with Megacam, CTIO DES, VISTA darkCAM, Pan-STARRS and LSST. A review of the various shear measurement methods is found in STEP2, along with their division into “active” and “passive” categories. Active techniques work by modelling galaxies as intrinsically circular, then

shearing the models until they most closely match the observed ellipticities. Passive methods work by measuring the apparent ellipticities of objects as well as higher order shape statistics, which are used to calibrate the ellipticities.

Flexion measurement methods are still in relative infancy. Initial attempts to mathematically describe the flexion distortion (Goldberg & Natarajan 2002; Irwin & Shmakova 2003) were formidably complicated. A passive estimator has been constructed by Okura, Umetsu & Futamase (2006); several important features in this approach remain to be developed, including PSF deconvolution and centroid-shifting. A completely different, probabilistic approach is taken by Irwin & Shmakova (2006) and Irwin, Shmakova & Anderson (2006). These approaches remain mathematically complex; it is therefore desirable to find a formalism which allows maximum physical insight into the problem. An advance towards this was made by Goldberg & Bacon (2005), who related flexion to the formalism of Cartesian shapelets (Refregier 2002; Refregier & Bacon 2002). Shapelets contain all the mechanics necessary to deconvolve galaxies and flexion estimators from the effects of a PSF. The active method of Goldberg & Bacon (2005) and Goldberg & Leonard (2006) has been used to successfully detect the flexion signal. The mathematics has a simpler form, although it is still not as elegant as possible.

Here, we present the image manipulations of lensing theory in terms of the “polar shapelets” formalism (Refregier 2001; Massey & Refregier 2005). This suggests a complete, orthonormal set of basis functions into which any galaxy shapes can be decomposed. It also provides a neat way to deconvolve arbitrary galaxy shapes from an arbitrarily complicated PSF, so we can set out under the assumption that this problem is solved. Polar shapelets then provide a natural representation for both shear and flexion operations, with simple mathematical forms that yield transparent physical interpretation. The complex number approach used throughout polar shapelets matches very conveniently with the complex ellipticity notation of Blandford (1991) now ubiquitous in shear literature, and with the complex formalism of flexion developed by Bacon *et al.* (2006). A complete software package to decompose images into polar shapelets is available from the shapelets web site<sup>\*</sup>.

We then exploit the inherent symmetries of polar shapelets to explore a comprehensive range of passive measurement methods for both shear and flexion. To create a shear or flexion estimator, we simply need to find a combination of shapelet coefficients that has the desired properties under each transformation. We generally keep the estimators as close as possible to linear in the image, to minimise both noise and bias in the final result. The shapelet methodology resembles a continuation of the KSB method to higher order. However, the inclusion of higher order shape information, and a complete parametrization of galaxy morphology, provides several new opportunities to improve on KSB, and to remove its instabilities. Some of the shear and flexion estimators that we describe are also independent, and can be obtained simultaneously for each galaxy. These will provide invaluable new cross-checks for systematics in the data analysis, which are unique to this method, and can also be combined to increase the overall ratio of signal to noise. As we shall discuss, one of the shear estimators has already been proved highly successful in a blind test on simulated images containing an applied shear, as part of the STEP programme (Heymans *et al.* 2006; Massey *et al.* 2006). We defer detailed testing of the remainder until the next STEP cycle.

This paper is organised as follows. In §2 we describe the shapelet decomposition and the action of weak gravitational lensing in shapelet space. In §3 we derive several possible weak shear estimators, and discuss the performance of a key estimator on the simulated STEP images. In §4 we derive several possible weak flexion estimators. We conclude in §5.

## 2 WEAK GRAVITATIONAL LENSING IN POLAR SHAPELET SPACE

We shall first describe the action of weak shears and weak flexions in polar shapelet space. This is seen as a mixing of power between an object’s various shapelet coefficients, or equivalently how much those coefficients change under each operation. To first order, a vector of shapelet coefficients is acted upon by simple matrices that contain small mixing components in their off-diagonal terms. For example, a shear takes some power from the circular ( $m = 0$ ) shapelet coefficients and redistributes it into the elliptical ( $m = 2$ ) shapelet coefficients, turning a circle into an ellipse.

The effect of shear as an abstract coordinate transformation has already been derived in Cartesian shapelet space by Refregier (2001), and in polar shapelet space by Massey & Refregier (2005). Here, we review this shear in the physical context of weak gravitational lensing. Operators to perform flexion have been derived in Cartesian shapelet space by Goldberg & Bacon (2005). Here, we translate those results into polar shapelet space, where they become much simpler. The flexion operators fit naturally into the complex notation of polar shapelets. Furthermore, the two distinct types of flexion identified by Bacon *et al.* (2006) mix distinct sets of polar shapelet coefficients, which can be separated elegantly.

### 2.1 Polar shapelet space in the absence of lensing

The observed image of every galaxy  $f(r, \theta)$  can be decomposed into a sum of (complex) orthogonal 2D basis functions  $\chi_{n,m}(r, \theta)$  weighted by (complex) shapelet coefficients  $f_{n,m}$

$$f(r, \theta) = \sum_{n=0}^{\infty} \sum_{m=-n}^n f_{n,m} \chi_{n,m}(r, \theta). \quad (1)$$

The basis functions, which are illustrated in figure 1, are fully described in Massey & Refregier (2005) and Bernstein & Jarvis (2002). They are Laguerre polynomials in  $r$  multiplied by sines and cosines in  $\theta$ , and a circular Gaussian of width  $\beta$ . This scale size is chosen to match the observed size of each galaxy, and the functions are placed at the galaxy’s centre of light. The shape of each galaxy can then be completely described by the array of its shapelet coefficients  $f_{n,m}$ . These are complex numbers, with  $f_{n,-m} = f_{n,m}^*$ . The indices  $n$  and  $m$  correspond to the numbers of radial and tangential oscillations respectively:  $n$  can take any nonnegative integer, and  $m$  can take any integer between  $-n$  and  $n$ , in steps of two. In practice, the expansion must be truncated, and we typically use coefficients with  $n$  less than some maximum amount or, conveniently in this context,  $n + |m|$  less than some amount. This is a cut in the *total* number of oscillations, so is more consistent with arguments concerning the information content in  $k$ -space, and also coincides more with the typical distribution of power in shapelet space. The index  $m$  will be the most significant in this paper, because coefficients with the same value of  $m$  describe features of a galaxy with the same degree of rotational symmetry.

In the absence of lensing, we first assume that galaxy shapes are randomly oriented. This must be true for a sufficiently large and

<sup>\*</sup> <http://www.astro.caltech.edu/~rjm/shapelets>

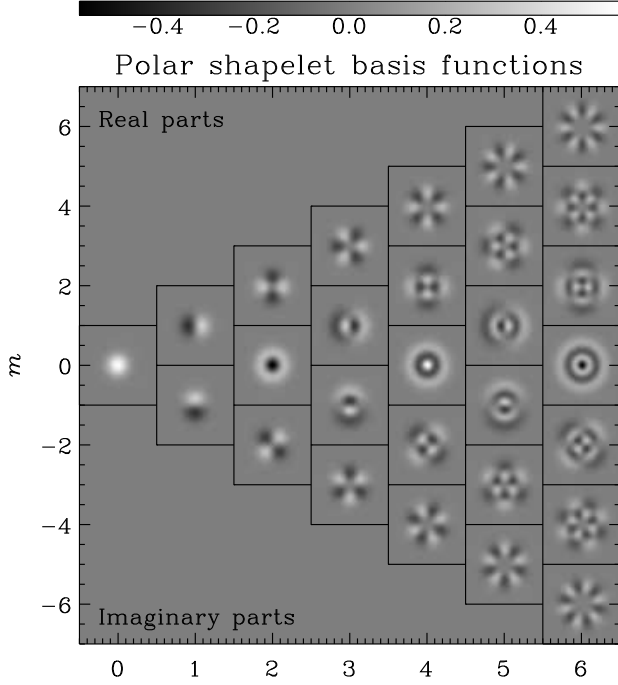


**Figure 1.** The polar shapelet basis functions, with indices  $n$  and  $m$  that describe the number of radial and tangential oscillations. The functions are complex, but several symmetries exist to ensure that a reconstructed image is wholly real, and these have been used to condense the plot. Basis functions (and shapelet coefficients) with opposite signs of  $m$  are complex conjugate pairs. Only the real part is shown here for basis functions with  $m \geq 0$  and the imaginary part for those with  $m < 0$ . The basis functions with  $m = 0$  are wholly real. The boxes have also been enlarged into the spaces between allowed coefficients for clarity.

widely-separated ensemble of galaxies, if there is no preferred direction in the universe, and if galaxies are not intrinsically aligned. The unlensed ensemble of galaxies can not contain any angular information, so must therefore have mean shapelet coefficients  $f_{nm}$  that obey

$$\langle f_{nm} \rangle = 0, \quad \text{if } m \neq 0. \quad (2)$$

Thus, only the  $m = 0$  coefficients of the ensemble average are populated. These encode the galaxies' average flux

$$F \equiv \iint f(r, \theta) r dr d\theta = \beta \sqrt{4\pi} \sum_n^{\text{even}} f_{n0}, \quad (3)$$

and the galaxies' average size

$$R^2 \equiv \frac{1}{F} \iint r^2 f(r, \theta) r dr d\theta = \frac{\beta^3 \sqrt{16\pi}}{F} \sum_n^{\text{even}} (n+1) f_{n0} \quad (4)$$

and radial profile (see Massey & Refregier 2005). This is the only information available about an unlensed galaxy ensemble, and all of it will be used later.

Although these will be zero on average for the population, we can also define an unweighted centroid

$$x_c \equiv \frac{1}{F} \iint r e^{i\theta} f(r, \theta) r dr d\theta = \frac{\beta^2 \sqrt{8\pi}}{F} \sum_n^{\text{odd}} \sqrt{n+1} f_{n1} \quad (5)$$

and ellipticity

$$\varepsilon \equiv \frac{1}{FR^2} \iint r^2 e^{2i\theta} f(r, \theta) r dr d\theta = \frac{\beta^3 \sqrt{16\pi}}{FR^2} \sum_n^{\text{even}} \sqrt{n(n+2)} f_{n2} \quad (6)$$

for each galaxy.

## 2.2 Effect of shear in shapelet space

As a bundle of light rays from a distant galaxy passes through a foreground gravitational field characterized by the lensing potential  $\Psi(x, y)$ , the rays are differentially deflected, and the apparent shape of the galaxy is distorted (*c.f.* Bartelmann & Schneider 2001). The shape of the galaxy  $f(x, y)$  is sheared by an amount

$$\gamma \equiv \gamma_1 + i\gamma_2 = \frac{1}{2} \left( \frac{\partial^2 \Psi}{\partial x^2} - \frac{\partial^2 \Psi}{\partial y^2} \right) + i \frac{\partial^2 \Psi}{\partial x \partial y}. \quad (7)$$

Positive values of the real part,  $\gamma_1$ , correspond to elongations of the galaxy along the  $x$ -axis and compressions along the  $y$ -axis. Positive values of the imaginary part,  $\gamma_2$ , correspond to elongations of the galaxy along the line  $y = x$  and compressions along the line  $y = -x$ . In both cases, negative values indicate the opposite. This complex shear notation (and an analogous form of complex ellipticity) is useful in weak lensing because both components are expected to be zero on average in the absence of a signal. In this case, a modulus-argument form for shear would have a zero modulus, but no well-defined angle. The complex form also arises very naturally in polar shapelet space.

As shown in Massey & Refregier (2005), under a weak lensing shear  $\hat{S}$  to first order, the shapelet coefficients  $f_{nm}$  transform as

$$\begin{aligned} \hat{S} : f_{n,m} \rightarrow f'_{n,m} = & f_{n,m} \\ & + \frac{\gamma}{4} \left\{ \sqrt{(n+m)(n+m-2)} f_{n-2,m-2} \right. \\ & \left. - \sqrt{(n-m+2)(n-m+4)} f_{n+2,m-2} \right\} \\ & + \frac{\gamma^*}{4} \left\{ \sqrt{(n-m)(n-m-2)} f_{n-2,m+2} \right. \\ & \left. - \sqrt{(n+m+2)(n+m+4)} f_{n+2,m+2} \right\} \end{aligned} \quad (8)$$

where the asterisk denotes complex conjugation. For an intrinsically circular galaxy, or a galaxy ensemble whose unlensed coefficients  $\langle f_{nm} \rangle$  obey equation (2), the lensed coefficients  $\langle f'_{nm} \rangle$  are left unchanged

$$\langle f'_{n,m} \rangle \simeq \langle f_{n,m} \rangle \quad \text{if } m \neq \pm 2, \quad (9)$$

except for the  $|m| = 2$  modes, where

$$\langle f'_{n,2} \rangle \simeq \frac{\sqrt{n(n+2)}}{4} \langle f_{n-2,0} - f_{n+2,0} \rangle \gamma, \quad (10)$$

with  $n = 2, 4, 6, \dots$ . After lensing, the galaxy has nonzero  $m = 0$  and  $|m| = 2$  coefficients (but no others). Figure 2 illustrates the action of mixing between nearby shapelet coefficients. The most obvious consequence is that the galaxy's unweighted ellipticity (6) also becomes non-zero. However, the fractional amount by which it changes depends upon the galaxy's radial profile. This idea will be explored in §3, along with other combinations of combinations of  $m = 2$  coefficients.

Note that even a pure shear can change the size of a galaxy, if it is not intrinsically circular. But propagating series (4) through operation (8), and comparing the result to series (6), it is easy to deduce that

$$\hat{S} : R^2 \rightarrow R'^2 = R^2 (1 + \gamma \varepsilon^* + \gamma^* \varepsilon) = R^2 (1 + 2\gamma_1 \varepsilon_1 + 2\gamma_2 \varepsilon_2). \quad (11)$$

In fact, there are (only) two different linear combinations of shapelet coefficients that are invariant under a first order shear:

$$\Gamma_1 = (4\pi)^{\frac{1}{2}}\beta \sum (f_{0,0} + f_{4,0} + f_{8,0} + \dots) \quad (12)$$

$$\Gamma_2 = (4\pi)^{\frac{1}{2}}\beta \sum (f_{2,0} + f_{6,0} + f_{10,0} + \dots). \quad (13)$$

Furthermore, their sum is the total flux  $F$ , whose measurement is also independent of the choice of scale size  $\beta$ .

### 2.3 Effect of second-order shear in shapelet space

The shear operator (8) is accurate only to first order. This is satisfactory in the normal regime of cosmic shear, for which  $|\gamma| \ll 1$ . To represent a full shear transformation

$$\begin{pmatrix} x' \\ y' \end{pmatrix} = \begin{pmatrix} 1 - \gamma_1 & -\gamma_2 \\ -\gamma_2 & 1 + \gamma_1 \end{pmatrix} \begin{pmatrix} x \\ y \end{pmatrix}, \quad (14)$$

requires additional terms of higher order in  $\gamma$ . These can be found by repeated application of operation (8). For example, applying the operator twice, with a shear each time of  $\gamma/2$ , adds mixing of order  $\gamma^2$  between coefficients whose  $n$  and  $m$  indices differ by 4. After many such operations, we fully exponentiate the shear operator in the way described in the appendix of Bernstein & Jarvis (2002). This practice should be used wherever possible in the implementation of shear transformations, and is done by default in the public code. In the context of shear measurement, it is merely interesting to note that the next shapelet coefficients to be affected in this way have  $m = 0$  or  $m = \pm 4$ . These coefficients are distinct from others that will be discussed in the context of all the other operations dealt with by this paper.

### 2.4 Effect of flexion in shapelet space

If the shear field varies significantly across the width of an object, one side is distorted more than the other, and it becomes bent into an arclet. This effect has been dubbed ‘‘flexion’’. Building upon the work of Goldberg & Bacon (2005), we shall now describe the distortions that arise from such gradients in the shear field,  $\frac{\partial\gamma}{\partial x}$ . The calculations will remain in the weak lensing regime, in the sense that no terms of order  $\gamma^2$  will be considered. However, flexion is most apparent along lines of sight close to foreground mass concentrations, where the shear is also likely to be strong. The more rapid falloff of a flexion signal as a function of distance from foreground mass can be used to probe smaller physical scales than a weak shear analysis, which produces relatively non-local mass reconstructions. Bacon *et al.* (2005) demonstrate that it can be used to more precisely measure substructure of dark matter halos, and their inner profile or concentration.

Bacon *et al.* (2005) pointed out that the flexion signal can be split into two separate (complex) terms, the first and second flexions

$$\mathcal{F} \equiv \left( \frac{\partial}{\partial x} - i \frac{\partial}{\partial y} \right) \gamma = (\gamma_{1,1} + \gamma_{2,2}) + i(\gamma_{2,1} - \gamma_{1,2}) \quad (15)$$

$$\mathcal{G} \equiv \left( \frac{\partial}{\partial x} + i \frac{\partial}{\partial y} \right) \gamma = (\gamma_{1,1} - \gamma_{2,2}) + i(\gamma_{2,1} + \gamma_{1,2}). \quad (16)$$

We assume that these have the same units as  $1/\beta$  which, in the public code, is always expressed in terms of image pixels. Via a derivation analogous to that in Cartesian space by Goldberg & Bacon (2005), we can determine the action of the flexion operators  $\widehat{\mathcal{F}}$  and  $\widehat{\mathcal{G}}$  in polar shapelet space. These are much simpler than corresponding expressions in Cartesian shapelet space, because distinct

sets of coefficients are coupled in polar shapelet space by the two operations, and the flexion also fits naturally into our current complex notation.

$$\begin{aligned} \widehat{\mathcal{F}} : f_{n,m} &\rightarrow f'_{n,m} = f_{n,m} \\ &+ \frac{\mathcal{F}\beta}{16\sqrt{2}} \left\{ 3\sqrt{(n-m)(n+m)(n+m-2)} f_{n-3,m-1} \right. \\ &\quad + (3n-m+10)\sqrt{(n+m)} f_{n-1,m-1} \\ &\quad - (3n+m-4)\sqrt{(n-m+2)} f_{n+1,m-1} \\ &\quad \left. - 3\sqrt{(n+m+2)(n-m+2)(n-m+4)} f_{n+3,m-1} \right\} \\ &+ \frac{\mathcal{F}^*\beta}{16\sqrt{2}} \left\{ 3\sqrt{(n+m)(n-m)(n-m-2)} f_{n-3,m+1} \right. \\ &\quad + (3n+m+10)\sqrt{(n-m)} f_{n-1,m+1} \\ &\quad - (3n-m-4)\sqrt{(n+m+2)} f_{n+1,m+1} \\ &\quad \left. - 3\sqrt{(n-m+2)(n+m+2)(n+m+4)} f_{n+3,m+1} \right\}, \end{aligned} \quad (17)$$

where the asterisk denotes complex conjugation. Similarly,

$$\begin{aligned} \widehat{\mathcal{G}} : f_{n,m} &\rightarrow f'_{n,m} = f_{n,m} \\ &+ \frac{\mathcal{G}\beta}{16\sqrt{2}} \left\{ \sqrt{(n+m)(n+m-2)(n+m-4)} f_{n-3,m-3} \right. \\ &\quad + \sqrt{(n+m)(n+m-2)(n-m+2)} f_{n-1,m-3} \\ &\quad - \sqrt{(n+m)(n-m+2)(n-m+4)} f_{n+1,m-3} \\ &\quad \left. - \sqrt{(n-m+2)(n-m+4)(n-m+6)} f_{n+3,m-3} \right\} \\ &+ \frac{\mathcal{G}^*\beta}{16\sqrt{2}} \left\{ \sqrt{(n-m)(n-m-2)(n-m-4)} f_{n-3,m+3} \right. \\ &\quad + \sqrt{(n-m)(n-m-2)(n+m+2)} f_{n-1,m+3} \\ &\quad - \sqrt{(n-m)(n+m+2)(n+m+4)} f_{n+1,m+3} \\ &\quad \left. - \sqrt{(n+m+2)(n+m+4)(n+m+6)} f_{n+3,m+3} \right\}. \end{aligned} \quad (18)$$

These operators are illustrated graphically in figure (2).

One crucial difference from the shear operator is that applying a flexion shifts the galaxy’s observed centroid (5) by an amount

$$\Delta = \frac{R^2}{4\beta} (6\mathcal{F} + 5\mathcal{F}^*\varepsilon + \mathcal{G}\varepsilon^*), \quad (19)$$

in units of  $\beta$ , with the real part corresponding to the  $x$  direction and the imaginary part to the  $y$  direction. The elements of expression (19) are easily understood in terms of shapelet coefficients. A galaxy’s centroid is constructed from its  $m = 1$  coefficients. These coefficients are altered during a first flexion  $\widehat{\mathcal{F}}$  if the galaxy has power in any  $m = 0$  (size  $R^2$ ) or  $m = 2$  (ellipticity  $\varepsilon$ ) coefficients. It is altered during a second flexion  $\widehat{\mathcal{G}}$  if it has power in any  $m = -2$  (complex conjugate of ellipticity  $\varepsilon^*$ ) coefficients. Its  $m = 4$  coefficients happen to cancel out in summation (5), and do not cause any shift. No comparable shift was introduced during shearing, so dealing with this will present a new technical challenge for weak lensing measurement.

Operators (17) and (18) are useful for applying an artificial flexion to an unlensed galaxy (for example, during the manufacture of simulated images). However, when galaxy shapes are measured, we shall assume that the shapelet decompositions are always centred around galaxies’ post-lensing centres of light (*i.e.* the observed centroid  $x_c = 0$ ); it being impossible to guess the original, pre-lensing sky position of the source. This point will be crucial in our later analysis because, for example, determinations of ellipticity and in particular  $\mathcal{F}$  depend strongly upon the origin of the coord-

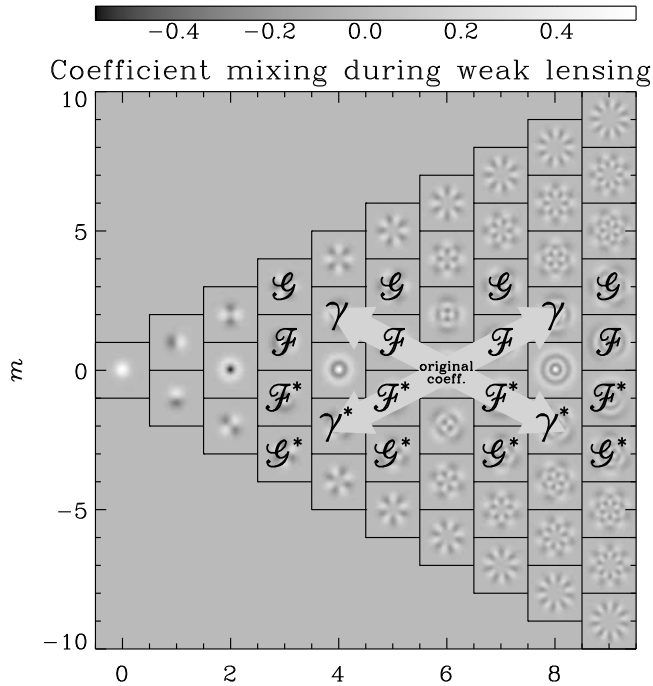


**Figure 2.** The mixing of polar shapelet coefficients under weak lensing transformations. If a galaxy initially contains power in its  $f_{6,0}$  coefficient, it will contain additional power in  $f_{4,\pm 2}$  and  $f_{8,\pm 2}$  after shear. After both types of flexion, it will contain additional power in eight shapelet coefficients, as illustrated. The directions in which power moves between adjacent coefficients are the same for a given operator wherever there are non-zero coefficients across shapelet space, although the amount of mixing varies. Wherever the pattern would seem to couple coefficients that do not exist, the amount of mixing is zero.

dinate system. To ensure that we account for this centroid shift, we are greatly aided by the linear dependence of (19) upon  $\mathcal{F}$  and  $\mathcal{G}$ : the change in coordinate frame can be simultaneously corrected for by simply including an appropriate translation in the flexion operator used for estimation

$$\widehat{\mathcal{F}}_{\mathcal{T}} \equiv \widehat{\mathcal{F}} - \widehat{\mathcal{T}} \left( \frac{R^2}{4\beta} (6\mathcal{F} + 5\mathcal{F}^* \varepsilon) \right), \quad (20)$$

$$\widehat{\mathcal{G}}_{\mathcal{T}} \equiv \widehat{\mathcal{G}} - \widehat{\mathcal{T}} \left( \frac{R^2}{4\beta} \mathcal{G} \varepsilon^* \right),$$

where, from Massey & Refregier (2005), the translation operator is

$$\begin{aligned} \widehat{\mathcal{T}}(\Delta) : f_{n,m} \rightarrow f'_{n,m} = f_{n,m} & \\ & + \frac{\Delta}{2\sqrt{2}} \left\{ \sqrt{(n+m)} f_{n-1,m-1} \right. \\ & \quad \left. - \sqrt{(n-m+2)} f_{n+1,m-1} \right\} \\ & + \frac{\Delta^*}{2\sqrt{2}} \left\{ \sqrt{(n-m)} f_{n-1,m+1} \right. \\ & \quad \left. - \sqrt{(n+m+2)} f_{n+1,m+1} \right\}. \end{aligned} \quad (21)$$

These practical flexion operations for analysis of observed images effectively isolate the observable, shape-changing part of the flexion transformation by subtracting off the centroid shift.

As described in Goldberg & Bacon (2005), for the purposes of constructing workable flexion estimators the ellipticity  $\varepsilon$  can be estimated from the lensed galaxy image even though this will it-

self have changed under shear: the change in the centroid shift this represents is higher-order, which can be seen from equation (19). If deemed necessary, an estimate of the ellipticity corrected for locally measured shear could even be used, as there is nothing to prevent the galaxy shear analysis from being independently performed prior to any flexion analysis. These operators will be used to form flexion estimators from observed galaxy shapes in §4.

## 2.5 Effect of convergence in polar shapelet space

Convergence changes a galaxy’s size and brightness. Actually measuring convergence is difficult because galaxies are intrinsically of very different sizes and magnitudes, and it is very hard to know what these quantities would have been before lensing, even statistically. (Measurements of shear and flexion are made possible by the statistical assumption that an unlensed population of galaxies would be round.) However, it is important to take account of the effect of convergence on these measurements, which is given by

$$\kappa = \frac{1}{2} \left( \frac{\partial^2 \Psi}{\partial x^2} + \frac{\partial^2 \Psi}{\partial y^2} \right) \quad (22)$$

Increases in apparent galaxy size potentially cause ellipticities to be measured in different parts of a galaxy’s profile - further towards the core or out in the wings. This is compensated for by the adaptative choice of the shapelet scale size  $\beta$  during the shapelet decomposition described in Massey & Refregier (2005). Indeed, the operators  $\hat{K}$  and  $\hat{S}$  are commutative. Changes in galaxy flux, or the averaging of shear estimators from bright and faint galaxies can be controlled by constructing estimators that are invariant to object flux. This is trivially implemented for all of the estimators discussed in this paper by dividing by the flux. This has little effect on their utility because the flux is invariant under a shear, and if a galaxy is bright enough for its ellipticity to be measured, it should be easy to also measure its flux without much noise. Furthermore, galaxies can be given different weights in an analysis if it is thought, for example, that the fainter or smaller objects provide less accurate shear estimators because pixellisation or convolution with the PSF have irreversibly destroyed shape information.

Note that this does not mean that the issues of “reduced shear” (Bartelmann & Schneider 2001) or indeed “reduced flexion” (*c.f.* Okura, Umetsu & Futamase 2006) have been solved. It is assumed throughout this paper that we can not measure the actual shear itself, but some combination of shear (or flexion) and convergence. This is because the size of an object,  $R^2$ , also changes during a pure shear or a pure flexion (proportionally to  $\gamma$  or  $\mathcal{F}$  or  $\mathcal{G}$  if the object is not perfectly circular to begin, and  $\gamma^2$  or  $\mathcal{F}^2$  or  $\mathcal{G}^2$  even if it is). For the unweighted shear estimator  $\hat{\gamma}_{\text{unweighted}}$ , which is described in §3.3, we actually measure  $\gamma/(1 - \kappa)$ , but the precise form for other shear estimators depends on the adopted weight functions. In fact, shapelets provides a convenient series expansion with which these can be calculated; a formidable exercise in real space.

## 2.6 Effect of convolution in polar shapelet space

It is customary in weak lensing methods to also describe the change in galaxies’ shapes during convolution with a telescope’s point spread function. In shapelet space, convolution is another simple matrix operation (Refregier & Bacon 2001). A detailed description will not be necessary here, because the galaxies can be automatically deconvolved from the PSF while their shapelet coefficients are being measured, using a procedure similar to, but more stable

than, a matrix inversion (Massey & Refregier 2005). This procedure produces a shapelet model describing the appearance of each galaxy before convolution. This potential hurdle in high precision shape measurement is therefore omitted from this paper as a separate, and essentially solved, problem.

### 3 SHEAR ESTIMATORS

To measure weak shear, we would like to construct some combination of each galaxy’s observed shape components that is related to the shear field it has experienced. The combination can be of arbitrary complexity. For individual galaxies, the measured quantity will inevitably be noisy, because galaxies have their own intrinsic shapes, which are changed only very slightly by weak lensing. However, we shall aim to construct a shear estimator  $\tilde{\gamma}$  for which

$$\langle \tilde{\gamma} \rangle = 0 \quad (23)$$

when averaged over a large galaxy ensemble in the absence of shear; and, more importantly,

$$\hat{S} : \tilde{\gamma} \rightarrow \tilde{\gamma} + \gamma \quad (24)$$

individually. As discussed in §2.1, the first condition is easy to achieve by making sure that (the numerator of)  $\tilde{\gamma}$  contains only shapelet coefficients with  $m \neq 0$ . The second, calibration of the shear estimator, ensures that the estimator is always unbiased

$$\langle \tilde{\gamma} \rangle = \gamma, \quad (25)$$

but this is notoriously difficult to satisfy (*c.f.* Bacon *et al.*, 2001; Erben *et al.*, 2001; Heymans *et al.*, 2005; Massey *et al.*, 2006). Our effort will primarily be directed here.

The easiest methodical approach towards a passive shear estimator is to first construct a “polarisation” estimator  $\tilde{p}$  with the same rotational symmetries as shear. We then need to calculate its “shear susceptibility”

$$P_{ij}^\gamma = \frac{\partial p_i}{\partial \gamma_j}, \quad (26)$$

so that

$$\hat{S} : \tilde{p}_i \rightarrow \tilde{p}_i + P_{ij}^\gamma \gamma_j. \quad (27)$$

The shear susceptibility can usefully be thought of as two complex numbers; one for each component of shear. However, it is more commonly expressed as a real,  $2 \times 2$  tensor and, for the sake of familiarity, we shall adopt that notation here. Its diagonal (real) terms describe the amount by which the polarisation will change under a shear. The off-diagonal (imaginary) terms describe a peculiar mixing by which a shear in one direction can affect the polarisation in a direction at  $45^\circ$ . This is introduced by complex galaxy morphologies when a galaxy’s isophotes are not concentric.

We can then construct a shear estimator

$$\tilde{\gamma}_i = (P^\gamma)_{ij}^{-1} \tilde{p}_j. \quad (28)$$

to make sure that indeed

$$\langle \tilde{\gamma}_i \rangle = \langle (P_{ij}^\gamma)^{-1} \tilde{p}_j + (P_{ij}^\gamma)^{-1} P_{ij}^\gamma \gamma_i \rangle \quad (29)$$

$$= \langle (P_{ij}^\gamma)^{-1} \tilde{p}_j \rangle + \langle \gamma_i \rangle \quad (30)$$

$$= \gamma_i. \quad (31)$$

where the random intrinsic ellipticities of galaxies ensure that the first term vanishes, and thus condition (25) is satisfied.

However, we immediately encounter three difficulties which account for most of the problems in the current generation of shear measurement methods:

- **$P^\gamma$  is noisy.** It is usually constructed from an object’s higher order shape moments, which are even harder to measure than the polarisation. Since this appears on the denominator, it dramatically increases the scatter of the shear estimator; and any ratio of quantities with Gaussian errors produces the extended wings of a Cauchy distribution.

- **$P^\gamma$  is a tensor.** The matrix inversion in equation (28) is unstable, except for circularly symmetric galaxies, or an unlensed population ensemble, in which case the off-diagonal elements are always zero. In all other cases, shearing in one direction mixes ellipticity from all other directions, and this must be unmixed.

- **$P^\gamma$  is required pre-shear.** Each galaxy is observable only after it has been lensed. Unfortunately, the shear susceptibility factor may change during shear, to first order in  $\gamma$  for most galaxies, and to second order for even circularly-symmetric ones.

One possible solution to all three difficulties is to average  $P^\gamma$  from a set of intrinsically similar galaxies, or to fit a value from a large galaxy ensemble as a function of other observables. This method ought to find a suitable, statistical value for all galaxies. The method diagonalises the shear susceptibility; reduces noise; and, if the population is so large that it contains effectively no coherent shear signal, satisfies the requirement for the pre-shear measurement. However, averaging over a large population of galaxies is inelegant, in the sense that shear estimators for individual galaxies are no longer self-contained. It also introduces new problems: the main issue being the practical identification of a set of intrinsically similar galaxies. Most observable properties of a galaxy do change during a shear, and grouping galaxies by these leads to “Kaiser flow” (Kaiser, 2000). The common challenge facing all modern shear measurement methods is to either understand Kaiser flow statistically, or to control shear susceptibility and thus avoid it. In appendix A, we show how measurements with one polarisation estimator can be averaged to avoid Kaiser flow, and maximise the weak lensing signal.

For the rest of this section, we shall construct progressively more elaborate polarisation estimators. We begin with simple forms that are very compactly represented in polar shapelet space. We gradually exploit the symmetries of shapelets to add features. These are helped by the compact shapelet notation, although the expressions do get more complicated. Which of these advanced shear estimators is most appropriate to a given data set will depend on the desired application, the image quality (for example, whether it was taken from the ground or in space), and the number of shapelet coefficients available for each galaxy.

#### 3.1 Gaussian-weighted quadrupole moment

We shall start with the simplest possible combination of shapelet coefficients that can be used to build a polarisation estimator. Recall that the first shapelet coefficients to be affected by a shear are those with  $|m| = 2$ . Like shear, these rotate as  $e^{-2\phi}$ , and they are therefore suitable for our purposes. The simplest possible polarisation estimator is simply the first shapelet coefficient with  $m = 2$ , *i.e.*  $\tilde{p} = f_{2,2}$ . This has shear susceptibility

$$P_{11}^\gamma = (f_{0,0} - f_{4,0})/\sqrt{2} - \sqrt{3}\text{Re}\{f_{4,4}\} \quad (32)$$

$$P_{22}^\gamma = (f_{0,0} - f_{4,0})/\sqrt{2} + \sqrt{3}\text{Re}\{f_{4,4}\} \quad (33)$$

$$P_{12}^\gamma = P_{21}^\gamma = -\sqrt{3}\text{Im}\{f_{4,4}\}. \quad (34)$$

In images from the Hubble Space Telescope COSMOS survey (Scoville *et al.*, 2006), for example,  $\langle |f_{4,4}|/f_{0,0} \rangle \approx 0.079$ , which is not entirely negligible at the desired level of precision. By averaging the components of  $P^\gamma$  from a sufficiently large population of observed galaxies, or fitting them as a function of other observables like galaxy size and magnitude, we can explicitly force the mean  $m = 4$  coefficients to be zero, and ensure that the measured  $m = 0$  coefficients are statistically corrected before shear. With this simplification, the shear susceptibility factor can then be trivially inverted, and we arrive at the shear estimator

$$\tilde{\gamma}_{\text{Gaussian}} = \frac{\sqrt{2} f'_{2,2}}{\langle f_{0,0} - f_{4,0} \rangle}. \quad (35)$$

This recovers the methods of RRG (excluding the smear correction) and Refregier & Bacon (2001), casting them into the more succinct framework of polar shapelets. It recovers KSB up to the normalisation of the polarisation estimator. To avoid biases and instability at low signal to noise, we have chosen to keep the polarisation and shear susceptibility linear in the image brightness. As a result however, both quantities vary widely in the full galaxy ensemble which typically encompass large ranges of flux and sizes, increasing the rate of Kaiser flow. A similar decision, *i.e.* whether to normalise by flux or not, will also have to be made for all of the following shear estimators.

### 3.2 Order-by-order shapelet shear estimator

A successful shapelet decomposition contains *all* of the available information about a galaxy's shape, and more information can be extracted than that available with previous shear estimators. Since *all* of the  $|m| = 2$  shapelet basis functions have the same rotational symmetries, each of the corresponding shapelet coefficients can be used to form independent<sup>†</sup> polarisation estimators  $p = f_{n,2}$ . These have shear susceptibilities

$$(P_n^\gamma)_{11} = \frac{1}{4} \left\{ \sqrt{n(n+2)} (f_{n-2,0} - f_{n+2,0}) + \sqrt{(n-4)(n-2)} \text{Re} \{f_{n-2,4}\} - \sqrt{(n+4)(n+6)} \text{Re} \{f_{n+2,4}\} \right\} \quad (36)$$

$$(P_n^\gamma)_{22} = \frac{1}{4} \left\{ \sqrt{n(n+2)} (f_{n-2,0} - f_{n+2,0}) - \sqrt{(n-4)(n-2)} \text{Re} \{f_{n-2,4}\} + \sqrt{(n+4)(n+6)} \text{Re} \{f_{n+2,4}\} \right\} \quad (37)$$

$$(P_n^\gamma)_{12} = (P_n^\gamma)_{21} = \frac{1}{4} \left\{ \sqrt{(n-4)(n-2)} \text{Im} \{f_{n-2,4}\} - \sqrt{(n+4)(n+6)} \text{Im} \{f_{n+2,4}\} \right\}, \quad (38)$$

which reduce to

$$P_n^\gamma = \frac{\sqrt{n(n+2)}}{4} \langle f_{n-2,0} - f_{n+2,0} \rangle \quad (39)$$

<sup>†</sup> Shapelet coefficients are independent in the absence of PSF deconvolution, but do become correlated if the PSF is of a similar size to the galaxy.

when averaged over an ensemble of galaxies as before. Thus, for each even order  $n$  available in a shapelet decomposition, we can construct one independent, unbiased shear estimator

$$\tilde{\gamma}_n = \frac{4}{\sqrt{n(n+2)}} \frac{f'_{n,2}}{\langle f_{n-2,0} - f_{n+2,0} \rangle}, \quad \text{for } n = 2, 4, 6, \dots \quad (40)$$

As before, these estimators are by construction unbiased, when averaged over the galaxy population.

One way to use these additional estimators is to diagnose problems in the measurement. Because we obtain multiple shear measurements for each galaxy after a *single* PSF deconvolution, their agreement provides a strong new test of systematics. If a pure shear signal is being successfully measured, all of the estimators from a given galaxy should average to the same value. However, if residual PSF effects are polluting the signal, the separate estimators will disagree. A weak lensing pipeline must be highly robust to pass such stringent tests, and they will provide a unique discriminatory power in future analyses. Although analogous tests could be constructed with active methods, they would not be as discriminating. For example, it would be possible to expand the definition of ‘‘circularity’’ in Bernstein & Jarvis (2002) to involve multiple shapelet coefficients. Unfortunately, this method performs shear estimation simultaneously with PSF deconvolution (and a complicated, non-linear iteration). Altering the shear estimator may also change any systematic influences, thus making it difficult to interpret any variation between the estimators.

Alternatively, the separate estimators can be linearly combined, with arbitrary weightings

$$p = \sum_{n=2}^{\infty} w_n f_{n,2}, \quad (41)$$

where the summation runs only over even indices  $n$ , for only those coefficients exist. In this case

$$P^\gamma = \sum_{n=0}^{\infty} w_n P_n^\gamma. \quad (42)$$

The weights  $w_n$  can be carefully constructed to optimise the signal-to-noise of the shear measurement (such as inverse variance weighting, as suggested by Refregier & Bacon 2001) or to remove systematic biases plaguing the particular data set. By staying linear in shapelet coefficients during this process, the polarisation and susceptibility also stay linear in the image, thus maintaining the stability of the shear estimator. In real space, changing the weights  $w_n$  is equivalent to changing the weight function used for the polarisation estimator. For the rest of this section, we shall explore various options for this weight function.

### 3.3 Unweighted quadrupole moment

One of the difficulties with general shear estimators, as described at the start of §3, is that they require the inversion of a (noisy) shear susceptibility tensor (42). This inversion is often unstable, and various implementations have chosen to either ignore the off-diagonal elements, or average over a large population of galaxies so that they disappear. The problem could be solved more easily if the shear susceptibility were explicitly a simple scalar (times the identity matrix) for each galaxy. Indeed, it is possible to weight the various orders of  $\tilde{\gamma}_n$  in such a way that the off-diagonal terms in their combined susceptibility tensor from successive orders cancel each other. The off-diagonal terms, and the differences between the on-diagonal terms, involve  $|m| = 4$  coefficients that are introduced

by the  $\gamma^*$  terms in equation (8). With these removed, the shear susceptibility (42) will only involve terms with  $m = 0$ . This can be trivially inverted.

A simple calculation to obtain the desired  $w_n$  yields

$$p = 4\sqrt{\pi}\beta^3 \sum_n \sqrt{n(n+2)} f_{n2}, \quad (43)$$

where the prefactor has been added to reproduce familiar quantities. In fact,  $p = FR^2\varepsilon$ , a version of the (radially) unweighted ellipticity without size (or flux) normalisation. Such polarisation has shear susceptibility

$$P^\gamma = 8\pi^{\frac{1}{2}}\beta^3 \sum_n (n+1)^{\frac{1}{2}} f_{n0} = FR^2. \quad (44)$$

A shear estimator can thus be formed

$$\tilde{\gamma}_{\text{unweighted}} \equiv \frac{\sum \sqrt{n(n+2)} f_{n2}}{2 \langle \sum \sqrt{(n+1)} f_{n0} \rangle}. \quad (45)$$

However, this estimator presents some unusual and intriguing problems. For previous shear estimators, we suggested that the shear susceptibility factor could be fitted as a function of the size and magnitude of each galaxy. Here, the shear susceptibility *is* the size and magnitude of each galaxy. As shown by equation (11), the size is changed during the shear. If the observed size is used, the mean shear from a population of galaxies can be forced to transform correctly, via a statistical “shear responsivity” calibration factor  $\mathcal{R} \equiv 2 - \langle \varepsilon^2 \rangle$  similar to that introduced by Bernstein & Jarvis (2002),

$$\tilde{\gamma}_{\text{unweighted}} \equiv \frac{\sum \sqrt{n(n+2)} f_{n2}}{(2 - \langle \varepsilon^2 \rangle) \sum \sqrt{(n+1)} f_{n0}}, \quad (46)$$

where the averaging is over a large population of galaxies.

This particular shear estimator emerged as one of the most successful shear measurement methods during blind tests as part of the STEP programme (Massey *et al.* 2006). This programme constructed simulated images that exhibit all the statistical properties of real astronomical images, but contain a known shear signal. While the measurement was performed (by JB), these input shears were kept hidden. They were then revealed publicly after all the pipelines had been run. Figure 3 shows the impressive performance of our  $\tilde{\gamma}_{\text{unweighted}}$  shear estimator for STEP2 image set A, which was specifically designed to mimic deep *Suprime-Cam* images from the *Subaru* telescope (Miyazaki *et al.*, 2002). A linear fit to these results shows a shear calibration factor (multiplicative measurement bias) of  $m = 0.023 \pm 0.029$  for the real component of shear, and  $m = 0.053 \pm 0.029$  for the imaginary component. There is no significant residual shear offset (additive measurement bias), with the fitted values being  $c = (-6.8 \pm 6.5) \times 10^{-4}$  for the real component of shear and  $c = (1.3 \pm 6.6) \times 10^{-4}$  for the imaginary component. This estimator demonstrated the best performance throughout the STEP2 project and, as suggested by that analysis, we shall reduce our error bars before the next round by incorporating a galaxy weighting scheme into our weak lensing pipeline.

One additional benefit of this estimator is that both the polarisation and the shear susceptibility are independent of the shapelet scale  $\beta$ . Although the ensemble average of any shear estimators  $\langle \tilde{\gamma}_n \rangle$  should always be independent of  $\beta$ , in general, individual estimators  $\tilde{\gamma}_n$  may not be. But in the current case, once a shapelet series has converged,  $F$ ,  $R^2$  and  $\varepsilon$  combine coefficients in such a way as to not depend upon the choice of  $\beta$  (Massey &

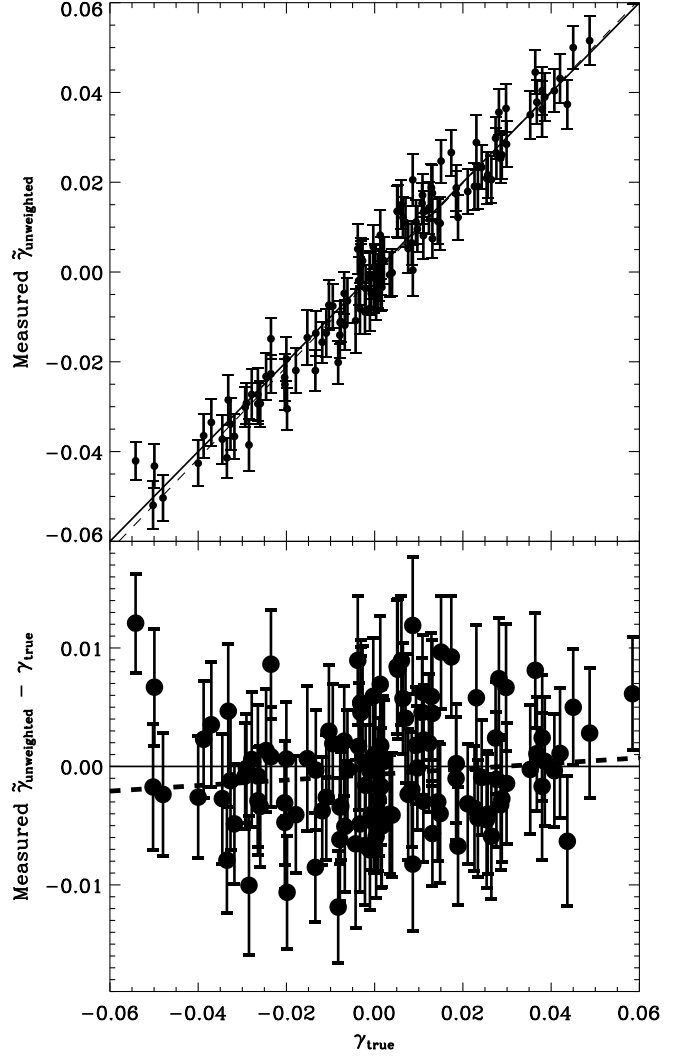


**Figure 3.** Performance of the shear estimator with an explicitly diagonal shear susceptibility tensor, on simulated images containing a known true shear. Points show both components of the mean shear, measured in  $7' \times 7'$  patches of sky where the input shear was held constant. For a perfect shear estimator, these would lie on the solid line. The dashed line is a linear fit to deviations from it.

Refregier, 2005). This result is non-trivial: in our image decomposition pipeline, we choose  $\beta$  to optimise the image reconstruction and stabilise the PSF deconvolution. However, this is only one possible goal. In IMCAT implementations of the KSB method, the equivalent of  $\beta$  is instead chosen to maximise the signal-to-noise for detection of the object. In SExtractor implementations of KSB, a scaling of SExtractor parameters is used. In all cases, the choice of  $\beta$  will also be affected by any applied shear that changes a galaxy’s apparent size. Whether this change is negligible depends on the specific implementation of the algorithm to determine  $\beta$  and must be tested experimentally. In this case, it is reassuring to note that this effect is formally absent, modulo the convergence of the series.

Since the STEP tests, we have also derived the full “Kaiser flow” behaviour of this estimator. This has a particularly interesting form, and is discussed fully in appendix A.

### 3.4 Using galaxies' radial profiles to reduce $\sigma_\gamma$

A galaxy's observed  $m = 2$  coefficients consist of intrinsic ellipticity, shear-induced ellipticity, and noise. For an individual galaxy, there is no way to tell what fraction of each is intrinsic, and what fraction is the signal. However, a shapelet decomposition contains a great deal more information about a galaxy's morphology that has not yet been tapped. In particular, it is the galaxy's intrinsic radial profile ( $m = 0$  coefficients) that contribute most to any change in observed ellipticity during a shear. Since the  $m = 0$  coefficients are typically much larger than any others, they are also, fractionally, the least changed themselves under a small shear. We shall therefore approximate the unlensed radial profile as the observed, measured radial profile. We can then work out the "radial profile" of  $m = 2$  coefficients that could possibly have been induced by lensing. Any component of the intrinsic ellipticity that does not have the appropriate "radial profile" cannot possibly have been induced by lensing and, for our purposes, can be ignored. Thus we reduce the contamination of intrinsic galaxy ellipticity in our shear estimators, to only include components of intrinsic ellipticity that happen to have the right profile.

We determine the required weights  $w_n$  by applying a unit shear to the rotationally-invariant part of a model, and find

$$\tilde{\gamma}_{\text{profile}} \equiv 4 \frac{\sum \sqrt{n(n+2)} (f_{n-2,0} - f_{n+2,0}) f_{n,2}}{\langle \sum n(n+2) (f_{n-2,0} - f_{n+2,0})^2 \rangle}, \quad (47)$$

where one factor in the denominator comes from the shear susceptibility factor and one from the weighted average. Of course, we have not taken measures to eliminate the  $|m| = 4$  and off-diagonal terms in the shear susceptibility factor. The shear susceptibility will therefore need to be fitted from a galaxy population as a function of size, magnitude and possibly radial profile. Several shapelet-based parameters to span morphology variation are suggested in §7 of Massey & Refregier (2005).

### 3.5 Shear-invariant shear susceptibility

The shear susceptibility can be further simplified, by continuing to add terms to the polarisation estimator. So far, we have used the  $|m| = 2$  coefficients, but no others. In fact, all shapelet basis functions with  $|m| = \{2, 6, 10, 14, \dots\}$  contain the rotational symmetries of shear; the higher order functions just contain additional symmetries as well. They can not be used as shear estimators by themselves but, because of this, it is possible to add them to the  $|m| = 2$  coefficients. The resulting polarisation estimator will stay linear in shapelet coefficients, linear in image flux, and keep all of the desired symmetries. Here we shall demonstrate how higher order shapelet coefficients can be used to "sweep" terms in the shear susceptibility down to  $m = 0$ , and construct a polarisation

$$p = \sum_{m=2,6,10,\dots}^{\infty} \sum_{n=2,4,6,\dots}^{\infty} w_{n,m} f_{n,m} \quad (48)$$

with any desired susceptibility factor.

We begin with the  $f_{2,2}$  polar shapelet coefficient. As shown in §3.1, this has a shear susceptibility involving  $f_{0,0}$ ,  $f_{4,0}$  and  $f_{4,4}$ . The weight on the  $f_{2,2}$  coefficient in  $p$  can be used to create any desired factor in front of the  $f_{0,0}$  term in  $P^\gamma$ . In §3.3, we added coefficient  $f_{6,2}$  in such a way to cancel out the  $f_{4,4}$  coefficient in the shear susceptibility. Instead, we shall now add an amount of  $f_{6,2}$  (then  $f_{10,2}$ ,  $f_{14,2}$ , etc) to shape the susceptibility's  $f_{4,0}$  (and  $f_{8,0}$ ,  $f_{12,0}$ ) terms in any way. Assuming extrapolation to infinite  $n$ ,

**Table 1.** Coefficient weights for the real part of the  $\tilde{\gamma}_{\text{shear-invariant}}$  shear estimator (equation 49). The imaginary part of this shear estimator involves complex conjugates of terms with every other value of  $m$ , but is most conveniently found by instead rotating the galaxies by  $45^\circ$  then calculating the real part a second time.

$n$	$m$	$w_{n,m}$	$n$	$m$	$w_{n,m}$
2	2	$\sqrt{2}$	6	6	$8/(3\sqrt{20})$
4	2	$\sqrt{2/3}$	8	6	$4/(3\sqrt{35})$
6	2	$\sqrt{4/3}$	10	6	$8/(3\sqrt{35})$
8	2	$\sqrt{4/5}$	12	6	$8/(3\sqrt{105})$
10	2	$\sqrt{6/5}$	14	6	$8/(3\sqrt{42})$
12	2	$\sqrt{6/7}$	10	10	$16/(15\sqrt{7})$
14	2	$\sqrt{8/6}$	12	10	$16/(15\sqrt{77})$
			14	10	$96/(15\sqrt{462})$
			14	14	$64/(7\sqrt{858})$

we can thus construct a polarisation estimator with arbitrary  $m = 0$  terms in its shear susceptibility tensor. However, it will also contain non-zero  $|m| = 4$  terms and off-diagonal elements.

Now consider the  $f_{6,6}$  polar shapelet coefficient. This has a shear susceptibility involving  $f_{4,4}$ ,  $f_{8,4}$  and  $f_{8,8}$  coefficients. This can be added to the polarisation with a weight arranged so that the three  $f_{4,4}$  terms in the shear susceptibility now cancel out. The  $f_{10,6}$  coefficient can then be added so that the four  $f_{8,4}$  terms cancel, and so on. This leaves 'dangling' terms in the shear susceptibility with  $|m| = 8$  (and due to series truncation, in practice, high  $n$ ). Successive additions of  $|m| = \{10, 14, 18, \dots\}$  terms to the polarisation can push these terms to higher and higher  $|m|$ . Since the magnitude of shapelet coefficients for real galaxies typically fall off rapidly with  $n$  and  $|m|$ , the contribution of any remaining dangling terms due to series truncation decreases during this process.

A second, interwoven combination of shapelet coefficients starting with  $f_{4,2}$ ,  $f_{8,2}$  and  $f_{8,6}$  can also be constructed, to make a completely separate polarisation whose shear susceptibility involves arbitrary contributions of only  $f_{2,0}$ ,  $f_{6,0}$ ,  $\dots$  coefficients.

We are now free to decide the most suitable form for the shear susceptibility, and can construct any appropriate polarisation estimator. It would be easiest to satisfy requirement (24) if  $P^\gamma$  did not change under shear. We could then use the observed (post-shear) value for each individual galaxy. The only two quantities (12) and (13) like this can clearly be constructed from these two interwoven combinations of shapelet coefficients. We shall construct the polarisation estimator with shear susceptibility  $\Gamma_1 + \Gamma_2 = F$ , where  $F$  is the flux. We claim that this is the most linear possible shear estimator (and possibly therefore the most robust). Clearly, any shear estimator must eventually be normalised so that the same shape is calculated for two (otherwise identical) galaxies of different brightnesses. The flux is the simplest, and most robustly measured normalisation, and the obvious choice to put on the denominator; *i.e.*

$$\tilde{\gamma}_{\text{shear-invariant}} \equiv \frac{1}{F} \sum_n \sum_m w_{n,m} f_{n,m}. \quad (49)$$

Calculating  $w_{n,m}$  for this case is an elementary but tedious procedure using the iterative method described above. The first terms are listed in table 1. A parallel derivation is performed in real space, to the point of obtaining the differential equations that are solved by this series expansion, in appendix B.

### 3.6 Convergence issues

Unweighted ellipticities (and higher-order properties) can not usually be measured from real images, due to the presence of noise that makes the integrals diverge. However, this becomes possible with shapelets (or IM2SHAPE or GALFIT) because a noise-free (and un-pixelated and deconvolved) model of the galaxy is reconstructed. For different weight functions, the question becomes one of the convergence of galaxies' radial profiles to zero at large radii, or in high order terms of a Taylor series. A galaxy with an exponential profile has polar shapelet coefficients  $f_{n,0} \propto n^{-2.5}$  for a well chosen  $\beta$ , and all of the shear estimators do converge. For a further discussion of the convergence of shapelet series, see Massey & Refregier (2005).

Furthermore, although polar shapelet coefficients can be measured to infinite  $n$  using the linear overlap method (see Massey & Refregier 2005) for idealised data, this is not the case using the now standard  $\chi^2$  fitting method (see also Kuijken 2006; Nakajima & Bernstein 2006), or in the presence of pixelisation or a PSF (Berry, Hobson & Withington 2004). We therefore need to ensure that sufficient coefficients can be measured, particularly for the elaborate polarisation estimators that converge more slowly. They may therefore require galaxies of slightly higher signal to noise and  $n_{\max}$ . This can be achieved by raising the magnitude or size cut in a lensing catalogue, although the extent to which this is necessary has to be determined by experiment. However, the more elaborate polarisation estimators have correspondingly simpler shear susceptibilities, which converge faster. As was the case for noise, the minimisation of truncation errors is particularly important in the denominator, and this may in fact prove to be the deciding factor.

### 3.7 Active shear estimators with polar shapelets

Bernstein & Jarvis (2002), Kuijken (2006) and Nakajima & Bernstein (2006) suggest a rather different philosophy for constructing shear estimators. Instead of measuring an observed polarisation, and calculating how that would have changed during shear, Kuijken (2006) assumes that all objects were intrinsically circular, then shear them (or their coordinate frame) until the models matches the data. Bernstein & Jarvis (2002) shear objects until they are circular. This makes for a simpler calculation because the shape of each object, including its higher order moments, is known well *before* the operation. A shear susceptibility factor is still needed (the calibration factor  $\mathcal{R}$  in equation (5.33) of Bernstein & Jarvis (2002)). In that case, it depends on the definition of circularity, and must be fitted or interpolated from a galaxy population as a function of other observables. In this respect, it offers no advantage over a shear susceptibility.

Shearing an intrinsically circular object can be done in either real space or shapelet space. In shapelet space, polar and Cartesian coefficients are equivalent, but we encourage the adoption of polar shapelets because of their elegance and simplicity. For example, the model of a circular galaxy occupies only the  $m = 0$  coefficients, and its sheared perturbation encroaches upon only a small number of additional coefficients.

The process inevitably involves a non-linear iteration to find the best-fitting parameters  $x_c$ ,  $\beta$ ,  $n_{\max}$  and  $\gamma$ . Bernstein & Jarvis (2002) and Nakajima & Bernstein (2006) return to the pixelated image at each iteration, vary the input shear, and perform a new shapelet decomposition. This continues until the object appears circular in a shear coordinate frame. However, attempts that we have made to mimic this non-linear process appear unstable at low

signal-to-noise. Also, at any given point during the iteration, is not clear what prescription one should adopt for which of the four parameters to adjust in order to improve the fit. Kuijken (2006) points out that it is not necessary to return to the pixelated image since, after the first decomposition, a complete representation of each object is available in shapelet space. This makes the process much faster. He uses a Newton-Raphson algorithm to find the best-fitting shear, and could easily use a shear operator that includes higher order terms (see §2.3), although this has not yet been implemented. This approach has clear parallels to our  $\hat{\gamma}_{\text{profile}}$  estimator, and the practical algorithm contains rather similar elements.

## 4 FLEXION ESTIMATORS

### 4.1 Gaussian-weighted flexion estimators

We shall now try to develop estimators for the weak lensing flexion, making use of our experience with the shear estimators, and drawing tight analogies. The simplest passive simple flexion estimator can be formed from a similar approach to that taken when constructing our KSB-like shear estimator  $\tilde{\gamma}_{\text{Gaussian}}$ . For that, we considered the Gaussian weighted quadrupole moments, which were the first perturbed under a shear. In this case, the shapelet coefficients primarily affected by first and second flexions, transform as

$$\begin{aligned} \widehat{\mathcal{F}}_{\mathcal{T}} : f_{1,1} \rightarrow f_{1,1} &+ \frac{\mathcal{F}\beta}{8} \left\{ 6 \left( 1 - \frac{R^2}{\beta^2} \right) f_{0,0} + 6 \frac{R^2}{\beta^2} f_{2,0} \right. \\ &\quad \left. - 6f_{4,0} - 5\sqrt{2}\varepsilon^* \frac{R^2}{\beta^2} f_{2,2} \right\} \\ &+ \frac{\mathcal{F}^*\beta}{8} \left\{ -5\varepsilon \frac{R^2}{\beta^2} (f_{0,0} - f_{2,0}) \right. \\ &\quad \left. + \sqrt{2} \left( 1 + 6 \frac{R^2}{\beta^2} \right) f_{2,2} - 3\sqrt{6} f_{4,2} \right\}, \\ \widehat{\mathcal{G}}_{\mathcal{T}} : f_{3,3} \rightarrow f_{3,3} &+ \frac{\mathcal{G}\beta}{8} \left\{ \varepsilon^* \frac{R^2}{\beta^2} (f_{4,2} - \sqrt{3} f_{2,2}) + \right. \\ &\quad \left. \sqrt{6} (f_{0,0} + f_{2,0} - f_{4,0} - f_{6,0}) \right\} \\ &+ \frac{\mathcal{G}^*\beta}{8} \left\{ 2\varepsilon \frac{R^2}{\beta^2} f_{4,4} - 2\sqrt{30} f_{6,6} \right\}. \end{aligned} \quad (51)$$

Therefore, the combinations

$$\tilde{\mathcal{F}}_{\mathcal{T}} = \frac{4\beta}{3} \frac{f_{1,1}}{\langle (\beta^2 - R^2) f_{0,0} + R^2 f_{2,0} - \beta^2 f_{4,0} \rangle} \quad (52)$$

and

$$\tilde{\mathcal{G}}_{\mathcal{T}} = \frac{4\sqrt{6}}{3\beta} \frac{f_{3,3}}{\langle f_{0,0} + f_{2,0} - f_{4,0} - f_{6,0} \rangle} \quad (53)$$

can be used as simple flexion estimators.

Note that the  $\varepsilon$ s in equations (50) and (51) refer to the pre-lensing ellipticity, and really do cancel out when averaging over a population of galaxies, even in the presence of a shear field. However,  $R^2$  changes during both shears (which will inevitably be present if a flexion is) and flexions, if an object is not circularly symmetric. In practice, occurrences of  $R^2$  could be replaced by  $R^2(1 - \langle \varepsilon^2 \rangle / 2)$ , as they were in §3.3. Alternatively, since the shear and flexion estimators can be found independently, it would not be difficult to first find the local shear signal, and estimate the apparent error in  $R^2$  from that in advance.

## 4.2 Order-by-order shapelet flexion estimators

For the small and faint galaxies that make up the majority of a weak lensing survey, it will be difficult to measure polar shapelet coefficients beyond the  $n = 6$  terms needed to estimate  $\tilde{\mathcal{G}}$  as described above. However, for those galaxies whose higher order shapes can be measured, it is possible to generalise the flexion estimators.

The terms in curly brackets in equations (50) and (51) effectively describe a flexion susceptibility factor, which we introduce by analogy with the shear susceptibility factor (27). We shall then be able to form flexion estimators

$$\tilde{\mathcal{F}}_n \equiv ((P_n^{\mathcal{F}})_{ij})^{-1} f_{n,1} \quad (54)$$

and

$$\tilde{\mathcal{G}}_n \equiv ((P_n^{\mathcal{G}})_{ij})^{-1} f_{n,m}. \quad (55)$$

The flexion susceptibility factors are real,  $2 \times 2$  tensors, and can be calculated using equations (17) and (18). The need to subtract away an estimate of the shift in the galaxy centroid due to the flexion itself, expressed by equations (20) and (21), necessarily complicates these expressions. However, this then describes the *measurable* effect of flexion on galaxy images. The first flexion susceptibility for general  $m = 1$  polar shapelet coefficients is

$$(P_n^{\mathcal{F}})_{11} + i(P_n^{\mathcal{F}})_{21} = \quad (56)$$

$$\begin{aligned} & \frac{\beta}{16\sqrt{2}} \left\{ 3\sqrt{n+1} \left[ (n-1)(f_{n-3,0} - f_{n+1,0}) + \right. \right. \\ & \quad \left. \left. (n+3)(f_{n-1,0} - f_{n+3,0}) \right] \right. \\ & \quad + 3\sqrt{(n-3)(n-1)(n+1)} f_{n-3,2} \\ & \quad + (3n+11)\sqrt{n-1} f_{n-1,2} \\ & \quad - (3n-5)\sqrt{n+3} f_{n+1,2} \\ & \quad - 3\sqrt{(n+1)(n+3)(n+5)} f_{n+3,2} \\ & \quad \left. + 2\frac{R^2}{\beta^2} (6+5\varepsilon)\sqrt{n+1}(f_{n+1,0} - f_{n-1,0}) \right. \\ & \quad \left. + 2\frac{R^2}{\beta^2} (6+5\varepsilon^*)(\sqrt{n+3}f_{n+1,2} - \sqrt{n-1}f_{n-1,2}) \right\} \end{aligned}$$

$$(P_n^{\mathcal{F}})_{22} + i(P_n^{\mathcal{F}})_{12} = \quad (57)$$

$$\begin{aligned} & \frac{\beta}{16\sqrt{2}} \left\{ 3\sqrt{n+1} \left[ (n-1)(f_{n-3,0} - f_{n+1,0}) + \right. \right. \\ & \quad \left. \left. (n+3)(f_{n-1,0} - f_{n+3,0}) \right] \right. \\ & \quad - 3\sqrt{(n-3)(n-1)(n+1)} f_{n-3,2}^* \\ & \quad - (3n+11)\sqrt{n-1} f_{n-1,2}^* \\ & \quad + (3n-5)\sqrt{n+3} f_{n+1,2}^* \\ & \quad + 3\sqrt{(n+1)(n+3)(n+5)} f_{n+3,2}^* \\ & \quad \left. + 2\frac{R^2}{\beta^2} (6-5\varepsilon^*)\sqrt{n+1}(f_{n+1,0} - f_{n-1,0}) \right. \\ & \quad \left. - 2\frac{R^2}{\beta^2} (6-5\varepsilon)(\sqrt{n+3}f_{n+1,2}^* - \sqrt{n-1}f_{n-1,2}^*) \right\}. \end{aligned}$$

The second flexion susceptibility for  $m = 3$  coefficients is

$$(P_n^{\mathcal{G}})_{11} + i(P_n^{\mathcal{G}})_{21} = \quad (58)$$

$$\begin{aligned} & \frac{\beta}{16\sqrt{2}} \left\{ \sqrt{(n+3)(n+1)(n-1)} f_{n-3,0} \right. \\ & \quad + \sqrt{(n+3)(n+1)(n-1)} f_{n-1,0} \\ & \quad - \sqrt{(n+3)(n+1)(n-1)} f_{n+1,0} \\ & \quad - \sqrt{(n+3)(n+1)(n-1)} f_{n+3,0} \\ & \quad + \sqrt{(n-7)(n-5)(n-3)} f_{n-3,6} \\ & \quad + \sqrt{(n-5)(n-3)(n+5)} f_{n-1,6} \\ & \quad - \sqrt{(n-3)(n+5)(n+7)} f_{n+1,6} \\ & \quad \left. - \sqrt{(n+5)(n+7)(n+9)} f_{n+3,6} \right. \\ & \quad + 2\frac{R^2}{\beta^2} \varepsilon (\sqrt{n-1}f_{n+1,2}^* - \sqrt{n+3}f_{n-1,2}^*) \\ & \quad \left. + 2\frac{R^2}{\beta^2} \varepsilon^* (\sqrt{n+5}f_{n+1,4}^* - \sqrt{n-3}f_{n-1,4}^*) \right\} \end{aligned}$$

$$(P_n^{\mathcal{G}})_{22} + i(P_n^{\mathcal{G}})_{12} = \quad (59)$$

$$\begin{aligned} & \frac{\beta}{16\sqrt{2}} \left\{ \sqrt{(n+3)(n+1)(n-1)} f_{n-3,0} \right. \\ & \quad + \sqrt{(n+3)(n+1)(n-1)} f_{n-1,0} \\ & \quad - \sqrt{(n+3)(n+1)(n-1)} f_{n+1,0} \\ & \quad - \sqrt{(n+3)(n+1)(n-1)} f_{n+3,0} \\ & \quad - \sqrt{(n-7)(n-5)(n-3)} f_{n-3,6}^* \\ & \quad - \sqrt{(n-5)(n-3)(n+5)} f_{n-1,6}^* \\ & \quad + \sqrt{(n-3)(n+5)(n+7)} f_{n+1,6}^* \\ & \quad \left. + \sqrt{(n+5)(n+7)(n+9)} f_{n+3,6}^* \right. \\ & \quad + 2\frac{R^2}{\beta^2} \varepsilon (\sqrt{n-1}f_{n+1,2} - \sqrt{n+3}f_{n-1,2}) \\ & \quad \left. + 2\frac{R^2}{\beta^2} \varepsilon (\sqrt{n+5}f_{n+1,4} - \sqrt{n-3}f_{n-1,4}) \right\}. \end{aligned}$$

In all four cases, the last six terms are complex, and the final two emerge from the shift in an object's apparent centroid during flexion.

We shall now consider options by which  $m = 1$  and  $m = 3$  coefficients of different orders  $n$  can be combined. We search for sophisticated combinations that produce flexion estimators with useful properties, analogous to those already created for shear estimators.

## 4.3 Using galaxies' radial profiles to improve flexion estimators

Exactly as was done for shear estimators in §3.4, it is possible to use knowledge of a galaxy's radial profile to restrict which component of its  $|m| = 1$  or  $|m| = 3$  polar shapelet coefficients could have been induced by flexion. Via a parallel derivation, we obtain flexion estimators

$$\tilde{\mathcal{F}}_{\text{profile}} \equiv \frac{16\sqrt{2}}{3\beta} \frac{\sum w_n f_{n,1}}{\langle \sum (w_n^2) \rangle}, \quad (60)$$

where

$$w_n = \sqrt{n+1}(n-1)(f_{n-3,0} + f_{n+1,0}) + \sqrt{n+1}(n+3)(f_{n-1,0} + f_{n+3,0}) + \frac{4R^2}{\beta^2} \sqrt{n+1}(f_{n+1,0} + f_{n-1,0}); \quad (61)$$

and

$$\tilde{\mathcal{G}}_{\text{profile}} \equiv \frac{16\sqrt{2} \sum w_n f_{n,3}}{\beta \left\langle \sum (w_n^2) \right\rangle}, \quad (62)$$

where

$$w_n = \sqrt{(n-3)(n-1)(n+1)} \times (f_{n-3,0} + f_{n-1,0} - f_{n+1,0} - f_{n+3,0}). \quad (63)$$

These are guaranteed to converge, and the estimator for the second flexion in particular should provide a very clean measurement with minimal noise.

#### 4.4 Diagonal flexion susceptibility

It might also be hoped that successive off-diagonal terms in the flexion susceptibility matrices could be made to cancel via a suitable weighting scheme  $w_n$ , as was possible for shear in §3.3. Unfortunately, due to the presence of the centroid-shifting correction so necessary for reliable flexion estimators, this is difficult; especially for the first flexion.

For the second flexion we can come tantalisingly close, and indeed if we only consider the *pure*  $\hat{\mathcal{G}}$  transformation of equation (18), the weighting scheme  $w_n = \sqrt{(n-1)(n+1)(n+3)}$  can be used to form a second flexion estimator

$$\tilde{\mathcal{G}}_{\text{diagonal}} \equiv \frac{2\sqrt{2} \sum \sqrt{(n-1)(n+1)(n+3)} f_{n,3}}{\beta \left\langle \sum (3n^2 - 4n + 15) f_{n,0} \right\rangle}. \quad (64)$$

The numerator is in fact the  $\beta$ -invariant quantity  $Q$  obtained by setting  $s = 4$  and  $m = 3$  in equations (56) and (58) of Massey & Refregier (2005). In real space, it is none other than

$$\delta\xi = \iint r^3 e^{3i\theta} f(r, \theta) r dr d\theta \quad (65)$$

(up to some overall normalisation factor), as used for HOLICS by Okura, Umetsu & Futamase (2006). However, the inclusion of terms from the flexion-induced centroid shift (20) results in off-diagonal elements in  $P^{\mathcal{G}}$  that cannot all be removed through any combination of the  $m = 3$  coefficients.

In the case of the first flexion, the prospects are worse: even if we could omit the  $\mathcal{T}$  part of a practical flexion operator (which, as will be discussed below, for  $\mathcal{F}$  we most certainly can not), a  $w_n$  capable of cancelling the off-diagonal terms in the susceptibility matrix has yet to be found by the authors. The complication arises from the mixing of power between  $\Delta m, \Delta n = \pm 1$  coefficients in the first flexion operation (17). Like a centroid shift, flexion causes power to leak between adjacent shapelet coefficients (*c.f.* figure 2). However, whereas the centroid shift involves only the single ladder-operator transformations  $\hat{a}_r^\dagger, \hat{a}_l^\dagger, \hat{a}_r$  and  $\hat{a}_l$  (see Refregier 2003), flexion always acts via combinations of three of these ladder operations, taking three steps but doubling back to move only one overall. Since  $\hat{a}_r^\dagger$  does not commute with  $\hat{a}_r$ , nor  $\hat{a}_l^\dagger$  with  $\hat{a}_l$ , each  $\Delta m, \Delta n = \pm 1$  term in equation (17) is in fact a combination of five separate contributions, each of which representing a different, independent path between the coefficients. Worst of all, each

path contributes a differing,  $n$ -dependant proportion of the overall transformation. This added level of complexity for the first flexion transformation therefore precludes any estimator of first flexion with vanishing off-diagonal terms in the susceptibility matrix.

The  $\beta$ -invariant quantity obtained by setting  $s = -1$  and  $m = 1$  in equations (56) and (58) of Massey & Refregier (2005) could be used to measure first flexion. Unfortunately, this quantity does not appear to have any other properties that are particularly interesting in the context of weak lensing.

#### 4.5 Active flexion estimators with polar shapelets

In a similar way to the active shear estimators, it is also convenient to use a shapelet representation when distorting a circular object (or possibly an object with both circular  $m = 0$  and elliptical  $|m| = 2$  components) by applying flexion until it matches the observed shape. Goldberg & Bacon (2005) suggested a prescription in Cartesian shapelets, which has been implemented by Goldberg & Leonard (2006), to fit the odd shapelet coefficients by perturbing the even ones. This results in a simple,  $\chi^2$  minimisation via matrix inversion. However, their approach is not perfectly clean. The even Cartesian shapelet coefficients mix a great deal of structure beyond the circularly symmetric and elliptical components. These are isolated using polar shapelets and, furthermore, so are the first and second flexion signals. By using polar shapelets, it is possible to fit  $\mathcal{F}$  and  $\mathcal{G}$  independently, from the  $|m| = 1$  and  $|m| = 3$  polar shapelet coefficients. Since the white image noise from a sky background is spread evenly across coefficients in a shapelet decomposition, using fewer coefficients will result in a cleaner fit, with improved signal to noise.

## 5 CONCLUSIONS

We have described the mechanics of weak gravitational lensing in terms of “polar shapelets” (Refregier 2003; Massey & Refregier 2005). This is a set of basis functions which can be used to parametrize images, in a way that appears convenient for both weak shear and flexion. The symmetries of polar shapelets are well-matched to those of lensing. For example, the complex notation of polar shapelet coefficients, where their modulus represents the amount of power, and their phase represents their orientation, mirrors that commonly used in the literature to define a complex ellipticity. In addition, polar shapelets act to simply encapsulate the ideas of weak flexion which have been recently developed.

The symmetries inherent to the polar shapelet formalism provide useful insight into the somewhat related symmetries of weak lensing distortions. We have exploited this relation to construct estimators that are able to simultaneously extract both the weak shear and flexion signal from the observed shapes of distant galaxies. We attempt to bypass some of the limitations of KSB and other shear measurement methods that were reviewed in STEP2. Adopting the classification scheme from that programme, we briefly discussed the recasting of alternative, “active” shear and flexion estimators into the polar shapelet formalism, and comprehensively explored the options available for “passive” shear and flexion estimators.

The Gaussian-weighted shear estimator  $\tilde{\gamma}_{\text{Gaussian}}$  recovers old methods like KSB and RRG, but in a compact form. The unweighted shear estimator  $\tilde{\gamma}_{\text{unweighted}}$  takes advantage of the noise-free shapelet reconstructions to simplify the shear susceptibility tensor into a scalar quantity. This is what KSB-era methods would have liked to do, but were unable to implement because of noise in

images. The simplification of the shear susceptibility is completed with  $\tilde{\gamma}_{\text{shear-invariant}}$ . With this, the shear susceptibility is simply the object's flux: a robustly measured quantity, and one that does not change during shear. There is also the option to reduce the rms shear noise due to intrinsic galaxy ellipticities using  $\tilde{\gamma}_{\text{profile}}$ . Analogous estimators for flexion also exist for most of these options.

Interestingly, our method permits several independent shear estimators and several flexion estimators to be obtained simultaneously for each galaxy. Because we calculate them following a *single* PSF deconvolution or non-linear iteration, their agreement (or otherwise) will provide a stringent new test for imperfect PSF modelling and other residual systematic effects. Such tests are unique to our approach, as the interpretation of analogous active shear estimators would be hindered by the need to perform a separate PSF deconvolution for each estimator, and possibly removing any shared defects.

We have demonstrated the performance of one of our key shear estimators via blind tests that were part of the Shear TEsting Programme (STEP; Massey *et al.*, 2006). We shall compare the practical performance of our remaining shear estimators in a future round of STEP simulations. We are also implementing an option to input a known flexion signal in the image simulation suite of Massey *et al.* (2004). We are planning a smaller-scale, flexion version of STEP, to test the performance of emerging weak flexion estimators, including the ones presented in this work as well as others presented elsewhere. In the mean time, a complete IDL software package capable of performing the shapelet image decomposition, including the weak lensing manipulation and analysis described in this paper, is available from the shapelets web site <http://www.astro.caltech.edu/~rjm/shapelets>.

## ACKNOWLEDGMENTS

The authors are pleased to thank Richard Ellis, Gary Bernstein, Sarah Bridle, Mandeep Gill, Dave Goldberg, Catherine Heymans, John Irwin, Mike Jarvis, Reiko Nakajima, Jason Rhodes, Nick Scoville, Marina Shmakova and Lisa Wright for their help. DB is supported by a PPARC Advanced Fellowship.

## REFERENCES

- Bartelmann M., Schneider P., 2001, *Physics Reports* 340, 2910  
 Bernstein G. & Jarvis M., 2002, *AJ* 123, 583  
 Bacon D., Goldberg D., Rowe B. & Taylor A., 2006, *MNRAS* 365, 414  
 Bacon D., Refregier A., Clowe D., Ellis R., 2001, *MNRAS* 325, 1065  
 Bacon D. & Taylor A., 2003, *MNRAS* 344 1307  
 Blandford R., Saust A., Brainerd T. & Villumsen J., 1991, *MNRAS* 251, 600  
 Bradač, M. *et al.*, 2005, *A&A* 437, 49  
 Chang T. & Refregier, A., 2004, *ApJ* 617, 794  
 Erben T., Van Waerbeke L., Bertin E., Mellier Y., Schneider P., 2001, *A&A* 366, 717  
 Goldberg D. & Bacon D., 2005, *ApJ* 619, 741  
 Goldberg D. & Leonard A., 2006, *ApJ* submitted (astro-ph/0607602)  
 Goldberg D. & Natarajan P., 2002, *ApJ* 564, 65  
 Hettterscheidt M. *et al.*, 2006, *A&A* submitted (astro-ph/0606571)  
 Heymans C. *et al.*, 2005, *MNRAS* 361, 160  
 Hirata C., Seljak U., 2003, *MNRAS* 343, 459  
 Hoekstra H. *et al.*, 2006, *ApJ* in press (astro-ph/0511089)  
 Irwin J. & Shmakova M., 2003 (astro-ph/0308007)  
 Irwin J. & Shmakova M., 2006, *ApJ* 645, 1  
 Irwin J., Shmakova M. & Anderson J., 2006, *ApJ* submitted (astro-ph/0607007)  
 Jarvis M., Jain B., Bernstein G. & Dolney D., 2005, *ApJ* in press (astro-ph/0502243)  
 Kaiser N., Squires G. & Broadhurst T., 1995, *ApJ* 449, 460  
 Kaiser N., 2000, *ApJ* 537, 555  
 Kuijken K., 1999, *A&A* 352, 355  
 Kuijken K., 2006, *A&A* submitted (astro-ph/0601011)  
 Massey R., Refregier A., Conselice C. & Bacon D., 2004, *MNRAS* 348, 214  
 Massey R. & Refregier A., 2005, *MNRAS* 363, 197  
 Massey R., Bacon D., Refregier A. & Ellis R., 2005, *MNRAS* 359, 1277  
 Massey R. *et al.*, 2006, *MNRAS* submitted  
 Miyazaki S. *et al.* 2002, *ApJL*, 580, 97  
 Okura Y., Umetsu K. & Futamase T. 2006, *ApJ* submitted (astro-ph/0607288)  
 Refregier A., 2003, *ARA&A* 41, 645  
 Refregier A., Rhodes J., & Groth E., 2002, *ApJL* 572, 131  
 Refregier A., 2003, *MNRAS* 338, 35  
 Refregier A. & Bacon D., 2003, *MNRAS* 338, 48  
 Rhodes J., Refregier A. & Groth E., 2001, *ApJ* 552, L85  
 Scoville N. *et al.*, 2006, *ApJ* in press  
 Schneider P. & Lombardi M., 2002, *A&A* submitted (astro-ph/0207454)  
 Schrabback T. *et al.*, 2006, *A&A* submitted (astro-ph/0606611)  
 Semboloni E. *et al.*, 2006, *A&A* 452, 51  
 Van Waerbeke L., Mellier Y., Hoekstra H., 2005, *A&A* 429, 75  
 Wittman D., Tyson, J. A., Margoniner V., Cohen J., Dell'Antonio I., 2001, *ApJL* 557, 89  
 Wittman D., Margoniner, V., Tyson J. A., Cohen J., Becker A., Dell'Antonio I., 2003, *ApJ* 597, 218  
 Wittman D. *et al.*, 2006, *ApJ* 643, 128

## APPENDIX A: KAISER FLOW

### A1 Population Response

In §3.3, we obtained expressions for unweighted, unnormalised second moments for each galaxy. We constructed an unnormalised size measure  $q_0 \equiv FR^2$  and two unnormalised polarisation components  $q_1 \equiv F\varepsilon_1$  and  $q_2 \equiv F\varepsilon_2$ , all of which have strong flux dependencies.

We must now find an estimator for the local shear on an image given these polarisations. If we were interested in a shear estimate for a single galaxy, we might argue that since the lensed quantities we measure are related to unlensed quantities by

$$q'_0 = q_0 + 2q_\beta\gamma_\beta \quad (\text{A1})$$

$$q'_\alpha = q_\alpha + 2q_0\gamma_\alpha, \quad (\text{A2})$$

with  $\alpha, \beta = 1, 2$ , we could use an estimator for the shear

$$\tilde{\gamma}_\alpha = \frac{\langle q'_\alpha \rangle}{2\langle q_0 \rangle}. \quad (\text{A3})$$

However, when we come to combining shear estimators from galaxies with different flux and size properties, this approach is not adequate. Firstly, it does not give a prescription for how to optimally combine the estimates from galaxies with very different flux and shape properties. Furthermore, it ignores the fact that, under shear, some galaxies will flow out of a cell containing galaxies at a given flux,  $q_0$  and ellipticity, while other galaxies will flow in - and these flows may not cancel; a weighting scheme should take account of this.

In seeking to address these issues, we closely follow the approach offered by Kaiser (2000; section 3.2), although the fact that we are dealing with unweighted moments simplifies our analysis.

We wish to obtain an estimator for the shear that takes into account the shear-induced flow of galaxies in the parameter space  $(F, q_0, q^2)$ , where  $F$  is the flux and  $q^2 = q_\alpha q_\alpha$  is an invariant measure of the ellipticity amplitude of an object. We will find it convenient to describe  $q_\alpha = q\hat{q}_\alpha$ , with the unit polarisation vector given by  $\hat{q}_\alpha = \{\cos \phi, \sin \phi\}$ , *i.e.*  $\phi$  gives the position angle of the galaxy. In this case we can describe a volume element for polarisation by  $qdq d\phi$ , or  $\frac{1}{2}d(q^2)d\phi$ .

Let us consider the distribution of galaxies in this parameter space. We will represent sheared distributions as primed quantities. If the number density in this parameter space is  $n$ , then we can describe the conservation of galaxies under shear by

$$n'(F', q'_0, q'^2, \phi') dF' dq'_0 d(q'^2) d\phi' = n(F, q_0, q^2, \phi) dF dq_0 d(q^2) d\phi. \quad (\text{A4})$$

Note that this differs from Kaiser's (2000) analysis in not requiring integration over distinct polarisabilities, as these polarisabilities are themselves given by  $q_0$  and  $q_\alpha$  in our case, due to using unweighted moments.

We now multiply both sides of this equation by  $W(F', q'_0, q'^2)q'_\alpha = W(F, q_0 + \delta q_0, q^2 + \delta q^2)(q_\alpha + \delta q_\alpha)$ , where  $W$  is an arbitrary function, and integrate over all variables. This will ultimately allow us to obtain a relation between the average polarisation, the distribution of galaxies, and the shear. Initially we find

$$\int dF' dq'_0 d(q'^2) d\phi' n' W(F', q'_0, q'^2) q'_\alpha = \int dF dq_0 d(q^2) d\phi n W(F + \delta F, q_0 + \delta q_0, q^2 + \delta q^2) (q_\alpha + \delta q_\alpha). \quad (\text{A5})$$

This can be simplified by noting that, because of the isotropy of the unsheared population,

$$\int dF dq_0 d(q^2) d\phi n W(F, q_0, q^2) q_\alpha = 0. \quad (\text{A6})$$

Making a Taylor expansion of the left hand side of equation (A5), we obtain

$$\int dF' dq'_0 d(q'^2) d\phi' n' W(F', q'_0, q'^2) q'_\alpha = \int dF dq_0 d(q^2) d\phi n \left( W \delta q_\alpha + \frac{\partial W}{\partial q_0} \delta q_0 q_\alpha + \frac{\partial W}{\partial (q^2)} \delta (q^2) q_\alpha \right). \quad (\text{A7})$$

If we note from equations (A1) and (A2) that  $\delta q_0 = 2q_0\gamma_\beta$ ,  $\delta q_\alpha = 2q_0\gamma_\alpha$ , and  $\delta(q^2) = 4q_0\gamma_\beta q_\beta$ , we can integrate the above expression by parts to obtain

$$\int dF' dq'_0 d(q'^2) d\phi' n' W(F', q'_0, q'^2) q'_\alpha = \int dF dq_0 d(q^2) d\phi W \left( 2nq_0\delta_{\alpha\beta} - 2q_\beta q_\alpha \frac{\partial n}{\partial q_0} - 4q_0 q_\beta q_\alpha \frac{\partial n}{\partial (q^2)} \right). \quad (\text{A8})$$

Since  $W(F', q'_0, q'^2) = W(F, q_0, q^2)$  to first order in the shear, we can omit it on both sides (we are free to do this as it is arbitrary), to obtain a relation between the mean of the sheared galaxies' polarisations, and the galaxy distribution function, sizes, and shapes

$$\int nq_\alpha dF dq_0 d(q^2) d\phi = \gamma_\beta \int \left\{ 2nq_0\delta_{\alpha\beta} - 2q_\beta q_\alpha \frac{\partial n}{\partial q_0} - 4q_0 q_\beta q_\alpha \frac{\partial n}{\partial (q^2)} \right\} dF dq_0 d(q^2) d\phi. \quad (\text{A9})$$

We can usefully write this in terms of an average only over position angles of galaxies. If we move to writing expressions in terms of the density

$$n(F, q_0, q^2) = \int d\phi n(F, q_0, q^2, \phi), \quad (\text{A10})$$

and note that the average over position angles  $\langle q_\beta q_\alpha \rangle = \frac{1}{2}q^2\delta_{\alpha\beta}$ , then we can write the average of  $q_\alpha$  over position angle only (*i.e.* at fixed  $F, q_0, q^2$ ) as

$$\langle q_\alpha \rangle_{F, q_0, q^2} = \gamma_\alpha \left[ 2q_0 - \frac{1}{n} \frac{\partial n}{\partial q_0} - \frac{2}{n} \frac{\partial n}{\partial (q^2)} q_0 q^2 \right], \quad (\text{A11})$$

where  $n$  is  $n(F, q_0, q^2)$  rather than  $n(F, q_0, q^2, \phi)$ . It will be useful to introduce the susceptibility  $P$ , where  $\langle q_\alpha \rangle_{F, q_0, q^2} = P(F, q_0, q^2)\gamma_\alpha$  with

$$P(F, q_0, q^2) = 2q_0 - \frac{1}{n} \frac{\partial n}{\partial q_0} - \frac{2}{n} \frac{\partial n}{\partial (q^2)} q_0 q^2. \quad (\text{A12})$$

We have therefore obtained the appropriate polarisation to use as a function of flux, size and shape for an ensemble of galaxies. Hence we can construct a shear estimator for galaxies in a particular small cell in  $(F, q_0, q^2)$  space

$$\hat{\gamma}_\alpha^{\text{cell}} = \frac{1}{NP} \sum_{\text{gals in cell}} q_\alpha, \quad (\text{A13})$$

where  $N$  is the number of galaxies in the cell in question. However, we would like an estimator which did not require the splitting of galaxies into cells in parameter space, and which optimally combines the estimators from different galaxies. We discuss this problem in the next section.

## A2 Optimal Weighting

Here we will discuss the optimal weighting of shear estimators for a spatial cell-average shear. Again, we are following the work of Kaiser (2000).

For our parameter-space cell shear estimate given in equation (A13) above, we can find the estimator variance

$$\langle (\hat{\gamma}^{\text{cell}})^2 \rangle = \frac{2}{N^2 P^2} \left\langle \left( \sum q_1 \right)^2 \right\rangle = \frac{1}{N^2 P^2} \langle \sum q^2 \rangle, \quad (\text{A14})$$

where the final equality assumes that galaxy polarisations are essentially uncorrelated in the weak shear regime. Thus we obtain

$$\langle (\hat{\gamma}^{\text{cell}})^2 \rangle = \frac{q^2}{NP^2}. \quad (\text{A15})$$

Since parameter-space cells provide shear estimates which are uncorrelated from cell to cell, the optimal weighting  $W_{\text{cell}}$  is proportional to  $1/\langle (\hat{\gamma}^{\text{cell}})^2 \rangle = NP^2/q^2$ , as then the overall estimator variance will be minimised. So the final total shear estimate for a small spatial aread will be given by

$$\begin{aligned} \hat{\gamma}_\alpha^{\text{total}} &= \frac{\sum_{\text{cells}} (NP^2/q^2) (\sum_{\text{gals in cell}} q_\alpha/NP)}{\sum_{\text{cells}} NP^2/q^2} \\ &= \frac{\sum_{\text{galaxies}} Q \hat{q}_\alpha}{\sum_{\text{galaxies}} Q^2}, \end{aligned} \quad (\text{A16})$$

where  $Q \equiv P/q$ .

## APPENDIX B: THE MOST NEARLY LINEAR SHAPE ESTIMATOR IN REAL SPACE

### B1 Simple polarisation estimators

The simplest polarisation estimator can be constructed for a galaxy image  $I(x, y)$  as

$$\tilde{p}_1 \equiv \frac{1}{F} \iint (x^2 - y^2) I(x, y) \, dx dy \quad (\text{B1})$$

$$\tilde{p}_2 \equiv \frac{1}{F} \iint 2xy I(x, y) \, dx dy, \quad (\text{B2})$$

where the flux  $F \equiv \iint I(x, y) \, dx dy$ . The diagonal components of the shear susceptibility tensor for this estimator take the simple form  $2R^2$  (evaluated without the weight), and we recover the shear estimator  $\tilde{\gamma}_{\text{unweighted}}$  from §3.5. The  $F$  factor could also have been incorporated directly into the shear susceptibility factor; then both terms are formally linear, and it is only at the point of forming a shear estimator that any ratios need to be taken.

If we ignore the correction for PSF convolution, the KSB method can also be recast in these simple terms. This requires Gaussian-weighted quadrupole ellipticities

$$\tilde{p}_1 \equiv \frac{1}{R^2} \iint (x^2 - y^2) e^{-\frac{x^2+y^2}{2r_g^2}} I(x, y) \, dx dy \quad (\text{B3})$$

$$\tilde{p}_2 \equiv \frac{1}{R^2} \iint 2xy e^{-\frac{x^2+y^2}{2r_g^2}} I(x, y) \, dx dy, \quad (\text{B4})$$

where

$$R^2 \equiv \iint (x^2 + y^2) e^{-(x^2+y^2)/(2r_g^2)} I(x, y) \, dx dy \quad (\text{B5})$$

and  $r_g$  is the scale size of a Gaussian weight function. This is introduced to make sure the integrals converge in a noisy image, and to eliminate the effects of neighbouring objects. Unfortunately, this weight function complicates the correction for the PSF, and makes the corresponding  $P^{\text{sh}}$  tensor messy (see equations (5-2) to (5-4) in KSB). Introducing a ratio of moments at this early stage reduces the dynamic range of the ellipticities and the shear susceptibility, but also exacerbates the noise. KSB also derive a correction for the effects of PSF convolution on a galaxy's shape, with this Gaussian and assumptions about the form of the PSF built-in.

### B2 General linear shape estimators

We can generalise this procedure by defining two arbitrary weight functions  $W_i(x, y)$ , with  $i \in \{1, 2\}$ , that can be used to define two linear polarisations

$$\tilde{p}_i \equiv \iint W_i(x, y) I(x, y) \, dx dy \quad (\text{B6})$$

The coordinate system is then distorted by a shear

$$\begin{pmatrix} x' \\ y' \end{pmatrix} = \begin{pmatrix} 1 + \gamma_1 & \gamma_2 \\ \gamma_2 & 1 - \gamma_1 \end{pmatrix} \begin{pmatrix} x \\ y \end{pmatrix} \quad (\text{B7})$$

and our shape estimators for the observed image become

$$\tilde{p}_i = \iint W_i(x, y) \left[ I(x, y) - \gamma_1 x \frac{\partial I}{\partial x} + \gamma_1 y \frac{\partial I}{\partial y} - \gamma_2 x \frac{\partial I}{\partial y} - \gamma_2 y \frac{\partial I}{\partial x} \right] dx dy. \quad (\text{B8})$$

Integrating each term by parts, and including a boundary condition on the rapid convergence of the image to zero at large radii, we

obtain

$$\begin{aligned} \tilde{p}_i &= p_i^{\text{int}} + \gamma_1 \iint \left[ x \frac{\partial W_i}{\partial x} - y \frac{\partial W_i}{\partial y} \right] I(x, y) \, dx dy \\ &\quad + \gamma_2 \iint \left[ x \frac{\partial W_i}{\partial y} + y \frac{\partial W_i}{\partial x} \right] I(x, y) \, dx dy. \end{aligned} \quad (\text{B9})$$

This pair of integrals, for each of the two weight functions, make up the four coefficients in the shear susceptibility tensor. This procedure can also be followed in polar coordinates, where we find

$$\begin{aligned} \tilde{p}_i &= p_i^{\text{int}} \\ &\quad + \gamma_1 \iint \left[ r \cos 2\theta \frac{\partial W_i}{\partial r} - \sin 2\theta \frac{\partial W_i}{\partial \theta} \right] I(r, \theta) \, r dr d\theta \\ &\quad + \gamma_2 \iint \left[ r \sin 2\theta \frac{\partial W_i}{\partial r} + \cos 2\theta \frac{\partial W_i}{\partial \theta} \right] I(r, \theta) \, r dr d\theta. \end{aligned} \quad (\text{B10})$$

### B3 Shear-invariant shear susceptibility

As was the case in section B1, it is always impossible to form a completely linear shear estimator, since bright galaxies would then yield larger shear estimators than faint ones; it will always be necessary to normalise a shear estimator by something proportional to the object's flux. However, we can construct one ellipticity for which the shear susceptibility tensor is diagonal and whose diagonal coefficients are *exactly equal to* that flux (this is equivalent to including a factor of  $1/F$  in an ellipticity estimator that has  $P^\gamma \equiv 1$ ). This will solve all three problems raised at the beginning of §3, because the flux is the most easily measured quantity of an object, the matrix inversion can be replaced by a division, and the flux is not changed under a shear (nor will the overall shear estimator be changed by lensing magnification).

To achieve this shear estimator with the desired integrals from equation (B9), we require

$$x \frac{\partial W_1}{\partial x} - y \frac{\partial W_1}{\partial y} = y \frac{\partial W_2}{\partial x} + x \frac{\partial W_2}{\partial y} = 1 \quad (\text{B11})$$

$$y \frac{\partial W_1}{\partial x} + x \frac{\partial W_1}{\partial y} = x \frac{\partial W_2}{\partial x} - y \frac{\partial W_2}{\partial y} = 0, \quad (\text{B12})$$

so that

$$\frac{\partial W_1}{\partial x} = \frac{x}{x^2 + y^2}, \quad \frac{\partial W_1}{\partial y} = \frac{-y}{x^2 + y^2} \quad (\text{B13})$$

$$\frac{\partial W_2}{\partial x} = \frac{y}{x^2 + y^2}, \quad \frac{\partial W_2}{\partial y} = \frac{x}{x^2 + y^2}, \quad (\text{B14})$$

or in polar coordinates

$$\frac{\partial W_1}{\partial r} = \frac{\cos(2\theta)}{r}, \quad \frac{\partial W_1}{\partial \theta} = -\sin(2\theta) \quad (\text{B15})$$

$$\frac{\partial W_2}{\partial r} = \frac{\sin(2\theta)}{r}, \quad \frac{\partial W_2}{\partial \theta} = \cos(2\theta). \quad (\text{B16})$$

These differential equations are solved by the series expansions in §3.5.

This paper has been produced using the Royal Astronomical Society/Blackwell Science L<sup>A</sup>T<sub>E</sub>X style file.